Spatio-Spectral Mixed-Effects Model for Functional Magnetic Resonance Imaging Data

Hakmook Kang [a] , Hernando Ombao [b] , Crystal Linkletter [c] , Nicole Long [d] & David Badre [e]

[a] Department of Biostatistics, Vanderbilt University, Nashville, TN, 37232

[b] Department of Statistics, University of California, Irvine, CA, 92697

[c] Center for Statistical Sciences, Brown University, Providence, RI, 02912

[d] University of Pennsylvania, Philadelphia, PA, 19104

[e] Department of Cognitive, Linguistic and Psychological Sciences, Brown University, Providence, RI, 02912

PLEASE SCROLL DOWN FOR ARTICLE

Spatio-Spectral Mixed-Effects Model for Functional Magnetic Resonance Imaging Data

Hakmook KANG, Hernando OMBAO, Crystal LINKLETTER, Nicole LONG, and David BADRE

The goal of this article is to model cognitive control related activation among predefined regions of interest (ROIs) of the human brain while properly adjusting for the underlying spatio-temporal correlations. Standard approaches to fMRI analysis do not simultaneously take into account both the spatial and temporal correlations that are prevalent in fMRI data. This is primarily due to the computational complexity of estimating the spatio-temporal covariance matrix. More specifically, they do not take into account multiscale spatial correlation (between-ROIs and within-ROI). To address these limitations, we propose a spatio-spectral mixed-effects model. Working in the spectral domain simplifies the temporal covariance structure because the Fourier coefficients are approximately uncorrelated across frequencies. Additionally, by incorporating voxel-specific and ROI-specific random effects, the model is able to capture the multiscale spatial covariance structure: distance-dependent *local* correlation (within an ROI), and distance-independent *global* correlation (between-ROIs). Building on existing theory on linear mixed-effects models to conduct estimation and inference, we applied our model to fMRI data to study activation in prespecified ROIs in the prefontal cortex and estimate the correlation structure in the network. Simulation studies demonstrate that ignoring the multiscale correlation leads to higher false positive error rates.

KEY WORDS: Brain imaging; Fourier transform; Local spatial covariance; Multiscale correlation; Spectrum.

1. INTRODUCTION

Functional magnetic resonance imaging (fMRI) is a powerful tool for investigating brain function. Typical fMRI data consist of a set of discrete time series measured on three-dimensional volume elements, called voxels. We consider an fMRI dataset from an experiment on frontal cortex function in the human brain, where the broader scientific interest is to investigate if the rostro-caudal axis of the frontal lobes is organized hierarchically, that is, if posterior regions are functionally subordinate to anterior regions. To this end, we take the important first step to examine how the mean activation level at prespecified regions of interest (ROIs) respond to tasks associated with one- or two-dimensional cues. Exploring patterns of activation, using both *local* (within-ROI) and *global* (between-ROIs) correlations in the data, will contribute to understanding of the function of the frontal cortex in the human brain.

Typical analyses of fMRI data, using normal linear models (known as general linear models in the neuroscience literature), ignore spatial correlation in estimating model parameters but partially incorporate the correlation into inference procedures, for example, through random field theory (Worsley et al. 1992). Ignoring intrinsic correlation may lead to misleading or erroneous conclusions. In particular, ignored spatial correlation will underestimate standard errors, leading to Type I errors in the presence of positive spatial correlation (Dubin 1988). In fMRI data, such positive spatial correlation in voxel-level analysis is expected because the response of a particular voxel is likely

to be very similar to the responses of its neighboring voxels within same ROI. This is problematic because test statistics across voxels would not be independent of each other. In the case of analysis at predefined ROIs, the time series in each ROI are typically averaged and the standard analysis is applied (AV-OLS), resulting in the same inferential problems as voxel-level analysis.

A significant amount of work has been done to model the temporal correlation in fMRI data: autoregressive order of q_1 ($\text{AR}(q_1)$) models by Bullmore et al. (1996), autoregressive moving average (ARMA) models by Locascio et al. (1997), and general linear models applied to smoothed time series data by Worsley and Friston (1995). Bullmore et al. (2001) proposed a wavelet approach for the purpose of resampling, but this approach could be extended to disentangle nonstationary temporal correlation in fMRI data analysis. However, much less work has been done to capture the spatial or spatio-temporal correlation. The most common approach to analyzing fMRI data is to fit a general linear model at each voxel after a series of preprocessing steps including scanner drift correction, motion correction, correction for cardiac and respiratory-related physiological noise, co-registration between the subject-specific anatomical and functional images, normalization to a common anatomical space (for multisubject analysis), and spatial smoothing (Huettel, Song, and McCarthy 2004). Recently, Zhu et al. (2009) proposed a new approach to characterize stochastic noise in magnetic resonance data, for example, noise from physiological processes and rigid body motion by using the Rician distribution.

On the spatio-temporal front, Katanoda, Matsuda, and Sugishita (2002) addressed spatial dependency by borrowing information from the six nearest neighboring voxels in three orthogonal directions while working in the Fourier domain. This short physical distance approach is similar to the one proposed

Hakmook Kang is at the Department of Biostatistics, Vanderbilt University, Nashville, TN 37232 (E-mail: *hakmook.kang@vanderbilt.edu*). Hernando Ombao is at the Department of Statistics, University of California, Irvine, CA 92697 (E-mail: *hombao@uci.edu*). Crystal Linkletter is at the Center for Statistical Sciences, Brown University, Providence, RI 02912 (E-mail: *crystal_linkletter@brown.edu*). Nicole Long is now a doctoral student at the University of Pennsylvania, Philadelphia, PA 19104 (E-mail: *niclong@sas.upenn.edu*). David Badre is at the Department of Cognitive, Linguistic and Psychological Sciences, Brown University, Providence, RI 02912. (E-mail: *david_badre@brown.edu*).

by Worsley et al. (1996), where data are spatially smoothed with a Gaussian kernel. Another type of smoothing technique proposed by Worsley et al. (2002) involves spatial smoothing of the sample autocorrelation. Bowman (2005) used a two-stage data-driven cluster analysis for spatio-temporal estimation and inference of localized brain activity. In related work, Bowman (2007) proposed a mixed-effects spatio-temporal model to disentangle spatial and temporal correlation in Positron Emission Tomography scan data. For the spatial correlation, a parametric structure was assumed and a functionally defined distance metric based on mean activity profiles was proposed. Ombao et al. (2008) used a spatio-spectral approach to take into account spatial and temporal correlations in brain signal data. The main idea of this approach was to employ location-dependent, that is, spatially varying, temporal spectrum to understand the underlying spatio-temporal processes. Perhaps most closely related to the model we develop, Lange and Zeger (1997) proposed an approach working in the Fourier frequency domain to address the temporal correlation in fMRI data. Estimation of regression coefficients was based on least squares while allowing the hemodynamic response function (HRF) to be different from voxel to voxel. For inference purposes, they estimate spatial correlation of the coefficients based on generalized least squares estimation. However, intrinsic spatial correlation is not incorporated into parameter estimation nor is the *global* correlation structure modeled. A general complex fMRI activation model that characterized voxels based on task-related magnitude and phase change in the complex-valued sampling space of MRI was proposed by Rowe (2005), which could be considered as another class of spatio-temporal model in the complex plane.

It should be noted that fully Bayesian approaches are also available to model spatial and temporal correlations in fMRI data. A Bayesian two-stage hierarchical model that captures only temporal correlation in the first stage and short- and long-range spatial correlation in the second stage was proposed by Bowman et al. (2008). Assuming equal correlation between all pairs of voxels within an anatomical region significantly reduces computational cost; however, it can oversimplify the spatial correlation structure. Genovese (2000) used a nonlinear Bayesian hierarchical model, which allowed the HRF to be different from voxel to voxel to indirectly accommodate spatial dependence. More generally, hierarchical multivariate conditionally autoregressive models have been the prevailing favorite for analyzing spatio-temporally correlated data (e.g., Carlin and Banerjee 2003). For fMRI data specifically, a Bayesian adaptive spatial smoothing approach was proposed by Yue, Loh, and Lindquist (2010) to capture nonstationary spatial correlation, where the Gaussian smoothing kernel varied across space and time. However, smoothing approaches are known to add spatial correlation on top of the underlying spatial correlation, which can make it even more difficult to disentangle spatial dependency in data. Even though spatial smoothing can improve signal-to-noise ratio, spatial resolution will decline as a result, which is a major benefit of using fMRI data to begin with.

In this article, we develop a statistical model for estimating activation in specific regions of interest while taking into account spatial and temporal correlation. Although the *global* correlation can be interpreted as the functional connectivity between the ROIs, our primary goal is not estimating the *global* correlation but estimating task-related activation patterns while properly adjusting for temporal, within-ROI, and between-ROIs correlations. To achieve these goals, we develop a model that includes both fixed and random terms. The fixed terms are used to estimate ROI-specific activation effects of stimuli. The random terms capture the temporal correlation (within a voxel), and the multiscale spatial correlation: *local* spatial correlation and *global* correlation. It is noteworthy that the term multiscale is used to indicate more than one scale. Modeling the global correlation structure allows for the possibility of a negative-valued correlation between ROIs and provides insight into the functional connectivity structure. Common approaches employing any spatial covariance function, for example, exponential, Gaussian, or Matérn family (Chilès and Delfiner 1999), to capture the global correlation cannot allow the correlation to be negative because spatial correlation is always assumed to be positive. We examine the validity of our model via two simulation studies and use it to investigate higher cognitive control function in the anterior premotor cortex (prePMD), the lateral prefrontal cortex (PFC), and the primary visual cortex. The later is believed to be implicated in the task though not with the higher cognitive control function.

2. METHODS

2.1 Overview of the Proposed Model

We now provide a brief overview of the elements in our proposed spatio-spectral mixed-effects model. First, we analyze the fMRI time series data in the Fourier (spectral) domain because the Fourier coefficients are approximately uncorrelated across frequencies. This offers substantial simplification of the covariance structure of the data and, thus, significantly reduces computational burden (which is perhaps historically one of the main barriers to fitting spatio-temporal fMRI models). Moreover, the spectral approach can flexibly model the temporal correlation structure because it does not require any parametric assumption about temporal correlation (e.g., autoregressive or moving average). In our analysis, following the general principles in Sun, Miller, and D'Esposito (2004), we examined two bands within the range 0–0.2 Hz. Second, we introduce both fixed and random effects for proper estimation and inference. The activation effect of a stimulus on a particular ROI will be modeled as a fixed effect and will be estimated by pooling information across all voxels within that ROI. Additionally, each voxel in an ROI will have its own voxel-specific effect, decomposed into an ROI-specific fixed effect plus a voxel-specific random deviation. The latter is used to model the *local* spatial correlation that is essential for providing efficient and correct estimates of ROI-specific stimulus effects on activation. Finally, each ROI will have its own random intercept, independent of the stimulus, which will be employed to model the covariance between ROIs. These terms will be used to assess *global* correlation, a measure of functional connectivity of the brain network, which is defined as the coherence between two time series (Muller et al. 2001). Here, coherence is computed separately for the real and imaginary parts. We further clarify the concept of multiscale spatial correlation in Figure 1: the *local* spatial correlation within each ROI is denoted by thin arrows while *global* correlation among ROIs is denoted by thick arrows in the figure.
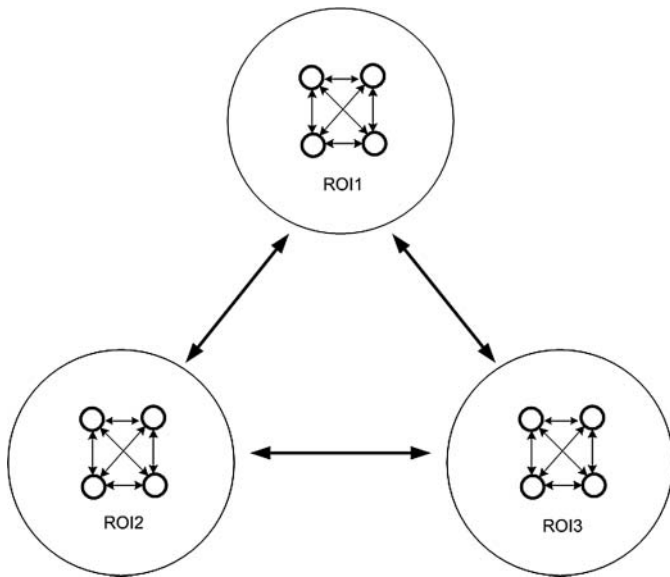
Figure 1. A schematic picture using three ROIs and four voxels per ROI illustrates the concept of multiscale correlations, that is, *local* correlation among voxels in an ROI denoted by thin arrows and *global* correlation among ROIs denoted by thick arrows.

2.2 Spatio-Spectral Mixed-Effects Model

We now develop our model in more detail. Suppose that there are P external stimuli, C many ROIs, and V_c many voxels within the cth ROI. We define $\psi_b(\cdot)$ and $\psi_d(\cdot)$ to be unspecified functions that generate valid covariance matrices, where only $\psi_b(\cdot)$ is a function of Euclidean distance. Define the time series at voxel v in ROI c to be $Y_{cv}(t)$, $t = 1, \ldots, T$. This would be the data typically observed in an fMRI study. Using a time domain model, we would need to consider three types of correlation, namely: (1) the local spatial correlation between voxels in the same ROI, (2) the correlation between different ROIs, and (3) the temporal correlation within a voxel.

Consider the following (time-domain) spatio-temporal mixed-effects model for the fMRI time series:

$$Y_{cv}(t) = \sum_{p=1}^{P} \left[\beta_c^p + b_{cv}^p\right] X_p(t) + d_c(t) + \epsilon_{cv}(t), \qquad (1)$$

where

- β_c^p is the ROI-specific activation level fixed effect due to stimulus p;
- b_{cv}^p is a zero-mean voxel-specific random deviation that accounts for the local spatial covariance between voxels within an ROI. Here, we specify the covariance structure to be

$$\mathbb{C}\text{ov}\left(b_{cv}^p, b_{c'v'}^p\right) = \begin{cases} \psi_b(\| v - v' \|) & \text{when } c = c', \\ 0 & \text{when } c \neq c'. \end{cases}$$

Note that when two voxels belong to different ROIs, then their corresponding b's are uncorrelated.

- $d_c(t)$ is a zero-mean ROI-specific signal with a covariance structure $\mathbb{C}\text{ov}(d_c(t), d_{c'}(t)) = \psi_d(c, c')$ that will be used to model connectivity across ROIs; and
- $\epsilon_{cv}(t)$ is the noise that takes into account temporal correlation within a voxel (conditional on ROI- and voxel-specific

random effects) under the separability and additivity assumptions regarding spatio-temporal correlation.

Our primary goal with this model is to make inferences with activation level, that is, linear combination of the β's, taking into account spatio-temporal correlation.

As might be obvious, the resulting correlation structure can be quite complex. However, the complexity in the spatio-temporal structure can be reduced by considering the analogue model in the frequency domain. The corresponding Fourier coefficient at the fundamental frequency $\omega_k = k/T$, where $k = 0, \ldots, T - 1$, of the observed fMRI time series $\{Y_{cv}(t), t = 1, \ldots, T\}$ is

$$Y_{cv}(\omega_k) = \sum_{t=1}^{T} Y_{cv}(t) \exp(-i2\pi \omega_k t).$$

Here, $Y_{cv}(\omega_k)$ is complex-valued with real and imaginary parts approximately uncorrelated under regularity conditions given in Shumway and Stoffer (2006). Although these conditions are difficult to confirm, they appear reasonable and have been employed in fMRI data analysis (e.g., Lange and Zeger 1997; Katanoda, Matsuda, and Sugishita 2002; Lazar 2008).

Define the Fourier coefficients of the other series $\{X_p(t)\}$, $\{d_c(t)\}$, and $\{\epsilon_{cv}(t)\}$ to be, respectively, $X_p(\omega_k)$, $d_c(\omega_k)$, and $\epsilon_{cv}(\omega_k)$, which are also all complex-valued. Since the Fourier transformation is a linear operator, the frequency-domain analogue of the model in Equation (1) is

$$Y_{cv}(\omega_k) = \sum_{p=1}^{P} \left[\beta_c^p + b_{cv}^p\right] X_p(\omega_k) + d_c(\omega_k) + \epsilon_{cv}(\omega_k). \quad (2)$$

Complexity of the covariance structure is reduced in the frequency domain because, under regularity conditions on the stationary error series $\{\epsilon_{cv}(t)\}$, the Fourier coefficients are approximately asymptotically uncorrelated across a prespecified set of Fourier frequencies (Brockwell and Davis 1991).

In practical fMRI data analysis, scientists are typically interested in a frequency band rather than a single frequency. Define $\boldsymbol{\Omega}_\ell$ to be a particular frequency band consisting of the set of frequencies $\{\pm\omega_1^\ell, \ldots, \pm\omega_{n_\ell}^\ell\}$ and denote the number of frequencies at band $\boldsymbol{\Omega}_\ell$ to be $N_\ell = 2n_\ell$. Some studies define $\boldsymbol{Y}_{cv}(\boldsymbol{\Omega}_\ell)$ to be the "response" vector for frequency band $\boldsymbol{\Omega}_\ell$,

$$\boldsymbol{Y}_{cv}(\boldsymbol{\Omega}_\ell) = \left[Y_{cv}(\omega_1^\ell), Y_{cv}(-\omega_1^\ell), \ldots, Y_{cv}(\omega_{n_\ell}^\ell), Y_{cv}(-\omega_{n_\ell}^\ell)\right]^T.$$

Let $\boldsymbol{\beta}_c = [\beta_c^1, \ldots, \beta_c^P]^T$ denote the fixed effects of the stimuli in ROI c; let $\boldsymbol{d}_c(\boldsymbol{\Omega}_\ell)$ and $\boldsymbol{b}_{cv} = [b_{cv}^1, \ldots, b_{cv}^P]^T$ be the ROI-specific random intercept and voxel-specific random effects due to external stimuli, respectively. We assume that the ROI-specific random effect depends on the frequency band, while the voxel-specific random effect is invariant to frequency. The parallel interpretation of this assumption in the time domain is from a multiscale correlation perspective, that is, *local* spatial correlation does not change over time but global correlation between ROIs can vary over time. Let $\boldsymbol{\epsilon}_{cv}(\boldsymbol{\Omega}_\ell)$ be a measurement error term at a voxel v in ROI c, which is parallel to the temporal correlation in the time domain. Then, we can express the response $\boldsymbol{Y}_{cv}(\boldsymbol{\Omega}_\ell)$ with a linear mixed-effects model at a frequency band $\boldsymbol{\Omega}_\ell$,

$$\boldsymbol{Y}_{cv}(\boldsymbol{\Omega}_\ell) = X(\boldsymbol{\Omega}_\ell)[\boldsymbol{\beta}_c + \boldsymbol{b}_{cv}] + \boldsymbol{d}_c(\boldsymbol{\Omega}_\ell) + \boldsymbol{\epsilon}_{cv}(\boldsymbol{\Omega}_\ell), \quad (3)$$

where $c = 1, \ldots, C$ is the index for the ROI and $v = 1, \ldots, V_c$ is the index for the voxel within ROI c. The dimensions of $\mathbf{Y}_c(\mathbf{\Omega}_\ell)$ for ROI c, $\mathbf{d}_c(\mathbf{\Omega}_\ell)$, and $\boldsymbol{\epsilon}_c(\mathbf{\Omega}_\ell)$ are $N_\ell V_c \times 1$, $\mathbf{X}(\mathbf{\Omega}_\ell)$ is $N_\ell V_c \times (V_c P)$, and $\boldsymbol{\beta}_c$ and $\mathbf{b}_c$ are $V_c P \times 1$. It is noteworthy that the elements of each vector $\boldsymbol{\beta}_c$ and $\mathbf{d}_c(\mathbf{\Omega}_\ell)$ are constant within an ROI. Let $d_c(\mathbf{\Omega}_\ell)$ denote the constant value of $\boldsymbol{d}_c(\mathbf{\Omega}_\ell)$.

2.2.1 Assumptions on the Spatio-Spectral Mixed-Effects Model (3). (A1.) The spatial process in each ROI is weakly stationary and isotropic, that is, $\mathbb{E}(\boldsymbol{Y}_{cv}(\mathbf{\Omega}_\ell))$ is constant within ROI c, and the covariance between any two voxels only depends on the Euclidian distance between the two voxels (Cressie 1993). That is, this model assumes local stationarity, which allows each ROI to have localized underlying spatial process.

(A2.) The three random terms, $d_c(\mathbf{\Omega}_\ell)$, $\boldsymbol{b}_{cv}$, and $\boldsymbol{\epsilon}_{cv}(\mathbf{\Omega}_\ell)$ are independent of each other and normally distributed: $\mathbf{d}(\mathbf{\Omega}_\ell) = \mathbf{d}^R(\mathbf{\Omega}_\ell) + i\mathbf{d}^I(\mathbf{\Omega}_\ell)$ in which $\mathbf{d}^j(\mathbf{\Omega}_\ell) = [d_1^j(\mathbf{\Omega}_\ell), \ldots, d_C^j(\mathbf{\Omega}_\ell)]^T \sim N_C(\mathbf{0}, \mathbf{\Sigma}_d^j(\mathbf{\Omega}_\ell))$, $j \in \{R, I\}$, where the superscripts R and I denote the real and imaginary part of complex number, respectively, and $N_q(\boldsymbol{\mu}, \mathbf{\Sigma})$ denotes the q-dimensional normal density with mean $\boldsymbol{\mu}$ and covariance matrix $\mathbf{\Sigma}$. In ROI c, $\mathbf{b}_c^p = [b_{c1}^p, \ldots, b_{cV_c}^p]^T \sim N_{V_c}(\mathbf{0}, \mathbf{\Sigma}_{bc}^p)$ for stimulus p. We denote the $n \times n$ identity matrix by $\mathbb{I}_n$, then $\boldsymbol{\epsilon}(\mathbf{\Omega}_\ell) = \boldsymbol{\epsilon}^R(\mathbf{\Omega}_\ell) + i\boldsymbol{\epsilon}^I(\mathbf{\Omega}_\ell)$ in which $\boldsymbol{\epsilon}^j(\mathbf{\Omega}_\ell) \sim N_{V_{tot}}(\mathbf{0}, (1/2)f(\mathbf{\Omega}_\ell)\mathbb{I}_{V_{tot}})$, $j \in \{R, I\}$, where $f(\mathbf{\Omega}_\ell)$ is the spectrum at frequency band $\mathbf{\Omega}_\ell$. Moreover, $\mathbf{b}_c^p$, $p = 1, \ldots, P$ are assumed to be independent of each other, $\mathbf{d}^R(\mathbf{\Omega}_\ell)$ is independent of $\mathbf{d}^I(\mathbf{\Omega}_\ell)$, and $[\boldsymbol{\epsilon}^R(\mathbf{\Omega}_\ell), \boldsymbol{\epsilon}^I(\mathbf{\Omega}_\ell)]^T \sim N_{2V_{tot}}(\mathbf{0}, \frac{1}{2}f(\mathbf{\Omega}_\ell)\mathbb{I}_{2V_{tot}})$, which is expected to hold when T is large (Shumway and Stoffer 2006).

(A3.) The covariance matrix $\mathbf{\Sigma}_{bc}$ for any external stimulus is assumed to encompass *local* spatial dependency between any pairs of voxels within ROI c:

$$\mathbb{C}\text{ov}\left(b_{cv}^p, b_{cv'}^p\right) = \sigma_{b^p c}^2 g(||v - v'||), \qquad (4)$$

where $\sigma_{b^p c}^2$ is the variance for the pth stimulus at any voxel within an ROI c, $g(\cdot)$ is an unspecified function, and $||v - v'||$ denotes Euclidian distance between two voxels v and v'. We estimate $g(\cdot)$ using the empirical variogram, which is a nonparametric method of estimating the spatial covariance matrix. Note that although we take a nonparametric approach to estimating $g(\cdot)$, one could use a parametric form such as exponential, Gaussian, or Matérn family (Chilès and Delfiner 1999). When looking at ROI c, it is assumed that $\mathbb{C}\text{ov}(b_{cv}^p, b_{c'v'}^p) = 0$ for $c \neq c'$. Finally, we assume that:

$$\mathbb{C}\text{ov}(d_c(\mathbf{\Omega}_\ell), d_{c'}(\mathbf{\Omega}_\ell)) = \mathbb{E}\{\mathbb{C}\text{ov}(\boldsymbol{Y}_{ci}(\mathbf{\Omega}_\ell), \boldsymbol{Y}_{c'j}(\mathbf{\Omega}_\ell))\} \quad (5)$$

for $c \neq c'$, where i and j indicate any voxels in clusters c and c', respectively. When $c = c'$, the variance is expressed as follows. Let $\boldsymbol{Z}_{cv}(\mathbf{\Omega}_\ell)$ denote $\boldsymbol{Y}_{cv}(\mathbf{\Omega}_\ell) - X(\mathbf{\Omega}_\ell)[\boldsymbol{\beta}_c + \mathbf{b}_{cv}]$. Then,

$$\begin{aligned} \mathbb{V}\text{ar}(d_c(\mathbf{\Omega}_\ell)) &= \mathbb{E}\{\mathbb{C}\text{ov}(\boldsymbol{d}_c(\mathbf{\Omega}_\ell) + \boldsymbol{\epsilon}_{cv}(\mathbf{\Omega}_\ell), \boldsymbol{d}_c(\mathbf{\Omega}_\ell) + \boldsymbol{\epsilon}_{cv'}(\mathbf{\Omega}_\ell))\} \\ &= \mathbb{E}\{\mathbb{C}\text{ov}(\boldsymbol{Z}_{cv}(\mathbf{\Omega}_\ell), \boldsymbol{Z}_{cv'}(\mathbf{\Omega}_\ell))\} \\ &\equiv \sigma_c^2. \end{aligned} \qquad (6)$$

The first equality holds due to the assumption that $\boldsymbol{d}_c(\mathbf{\Omega}_\ell)$ is independent of $\boldsymbol{\epsilon}_{cv}(\mathbf{\Omega}_\ell)$ and $\boldsymbol{\epsilon}_{cv}(\mathbf{\Omega}_\ell)$ is independent of $\boldsymbol{\epsilon}_{cv'}(\mathbf{\Omega}_\ell)$ for any voxels v and v' in ROI c if $v \neq v'$. The second equality is simply due to the definition of $\boldsymbol{Z}_{cv}(\mathbf{\Omega}_\ell)$.

Employing the spectral approach simplifies the spatio-spectral covariance structure because the covariance matrix of

a prespecified number (independent of T) of the Fourier coefficients is approximately diagonal. As a consequence, it allows us to fit spatio-spectral models with much reduced computational complexity compared to a time domain approach. Moreover, spectral analysis relaxes assumptions about the temporal correlation structure that are commonly required in time domain analysis, for example, a parametric assumption such as AR. However, as pointed out in the discussion of Lange and Zeger (1997), the spectral approach may not be ideal for analyzing fMRI data resulting from an event-related design. We believe though that it could still work for short block designs.

3. ESTIMATION AND INFERENCE

We first define some notations and operators. Define stc to be an operator that horizontally appends two matrices that have the same dimension in row. For ease in exposition, Model (3) is rewritten at a frequency ω instead of a frequency band Ω_ℓ by using matrix notation,

$$\boldsymbol{Y}(\omega) = \boldsymbol{X}(\omega)[\boldsymbol{\beta} + \boldsymbol{b}] + \boldsymbol{K}\boldsymbol{d}(\omega) + \boldsymbol{\epsilon}(\omega), \quad \text{where} \qquad (7)$$

- $\boldsymbol{Y}(\omega) = [Y_{11}(\omega), \ldots, Y_{1V_1}(\omega), Y_{21}(\omega), \ldots, Y_{CV_C}(\omega)]^T$ is a $V_{tot} \times 1$ response vector at a frequency ω;
- $\boldsymbol{X}(\omega) = stc(\mathbb{I}_{V_{tot}} \otimes X_1(\omega), \ldots, \mathbb{I}_{V_{tot}} \otimes X_P(\omega))$ in which $X_p(\omega)$ is the convolution between the p impulse function and the HRF;
- $\boldsymbol{\beta} = [\boldsymbol{\beta}^1, \boldsymbol{\beta}^2, \ldots, \boldsymbol{\beta}^P]^T$ is $V_{tot} P \times 1$ vector where $\boldsymbol{\beta}^p = [\beta_1^p, \ldots, \beta_1^p, \beta_2^p, \ldots, \beta_2^p, \ldots, \beta_C^p]^T$ for $p \in \{1, \ldots, P\}$;
- $\boldsymbol{b} = [\boldsymbol{b}^1, \boldsymbol{b}^2, \ldots, \boldsymbol{b}^P]^T$ is $V_{tot} P \times 1$ vector where $\boldsymbol{b}^p = [b_{11}^p, b_{12}^p, \ldots, b_{1V_1}^p, b_{21}^p, \ldots, \ldots, b_{CV_C}^p]^T$ for $p \in \{1, \ldots, P\}$;
- $\boldsymbol{K} = \boldsymbol{K}_1 \oplus \boldsymbol{K}_2 \oplus \cdots \oplus \boldsymbol{K}_C$, where $\oplus$ denotes direct sum and $\boldsymbol{K}_j$ is a vector of length V_j whose elements are all one, $j = 1, \ldots, C$, and $\boldsymbol{d}(\omega) = [d_1(\omega), \ldots, d_C(\omega)]^T$; and
- $\boldsymbol{\epsilon}(\omega) = [\epsilon_{11}(\omega), \ldots, \epsilon_{1V_1}(\omega), \epsilon_{21}(\omega), \ldots, \epsilon_{CV_C}(\omega)]^T$.

Due to the fact that $\boldsymbol{Y}(\omega)$ is approximately uncorrelated with $\boldsymbol{Y}(\omega')$ where $\omega \neq \omega'$, each $\boldsymbol{Y}(\omega)$, $\omega \in \{\omega_1^\ell, \ldots, \omega_{n_\ell}^\ell\}$ can be treated as an uncorrelated response vector.

3.1 Estimation of $\boldsymbol{\beta}$, $\mathbf{b}$, and $\mathbb{C}\text{ov}(\mathbf{b})$

Suppose that we have M many frequency bands and a band $m \in \{1, \ldots, M\}$ consists of n_m Fourier frequencies. Define a voxel-specific random term $\boldsymbol{\gamma}_{cv} = [\gamma_{cv}^1, \ldots, \gamma_{cv}^P]^T$ where $\gamma_{cv}^p = [\beta_c^p + b_{cv}^p]$. Then, by following the matrix notation, $\boldsymbol{\gamma} = \boldsymbol{\beta} + \mathbf{b}$. Conditioning on $\mathbf{b}$ and $\mathbf{d}(\omega)$, $\mathbb{E}(\boldsymbol{Y}(\omega)|\mathbf{b}, \mathbf{d}(\omega)) = \boldsymbol{X}(\omega)\boldsymbol{\gamma} + \mathbf{d}(\omega)$ and $\mathbb{V}\text{ar}(\boldsymbol{Y}(\omega)|\mathbf{b}, \mathbf{d}(\omega)) = f(\omega)\mathbb{I}_{V_{tot}}$, which provides a theoretical justification for using an Ordinary Least Square (OLS) estimator for $\boldsymbol{\gamma}$. The unconditional mean and variance are $\mathbb{E}(\boldsymbol{Y}(\omega)) = \boldsymbol{X}(\omega)\boldsymbol{\beta}$ and $\mathbb{V}\text{ar}(\boldsymbol{Y}(\omega)) \equiv \boldsymbol{\Gamma}(\omega) = \boldsymbol{X}(\omega)\mathbf{\Sigma_b}\boldsymbol{X}^T(\omega) + \boldsymbol{K}\mathbf{\Sigma_d}(\omega)\boldsymbol{K}^T + f(\omega)\mathbb{I}_{V_{tot}}$, where $\mathbf{\Sigma_b}$ is a block diagonal matrix that can be expressed as the direct sum of the spatial covariance matrices of $\mathbf{b}$ for each stimulus: $\mathbf{\Sigma_b} = \mathbf{\Sigma}_b^1 \oplus \mathbf{\Sigma}_b^2 \oplus \cdots \oplus \mathbf{\Sigma}_b^P$. Moreover, each $\mathbf{\Sigma}_b^p$ is also a block diagonal matrix because we assume that the voxel-specific random effect due to a stimulus p in ROI c is independent from that in ROI c' when $c \neq c'$. Therefore, $\mathbf{\Sigma}_b^p$ can also be expressed as the direct sum of the spatial covariance matrices for the random

effects in each ROI corresponding to external stimulus p, that is, $\boldsymbol{\Sigma}_b^p = \boldsymbol{\Sigma}_{b1}^p \oplus \boldsymbol{\Sigma}_{b2}^p \oplus \cdots \oplus \boldsymbol{\Sigma}_{bC}^p$.

The OLS estimator of $\boldsymbol{\gamma}$ is

$$\widetilde{\boldsymbol{\gamma}} = \left[\sum_{i=1}^{M} \boldsymbol{X}^T(\boldsymbol{\Omega}_i)\boldsymbol{X}(\boldsymbol{\Omega}_i) \right]^{-1} \left[\sum_{i=1}^{M} \boldsymbol{X}^T(\boldsymbol{\Omega}_i)\boldsymbol{Y}(\boldsymbol{\Omega}_i) \right]. \quad (8)$$

Then, by definition, $\widetilde{\boldsymbol{\gamma}} = \boldsymbol{\beta} + \mathbf{b}$ in which $\widetilde{\boldsymbol{\gamma}}$ and $\boldsymbol{\beta}$ play the role of a response and independent variable, respectively, in a regression framework. We apply iterative generalized least squares as described below to estimate $\boldsymbol{\beta}$ and the spatial covariance for $\mathbf{b}$, which is less computationally demanding than direct optimization of the likelihood function.

Step 1. Estimate $\boldsymbol{\beta}$ given $\boldsymbol{\Sigma}_\mathbf{b} = \mathbb{I}_{PV_{\text{tot}}}$. Define a column vector with a length V_c, $\boldsymbol{\xi}_c = [1, \ldots, 1]^T$ where $c = 1, \ldots, C$. Construct a matrix $\boldsymbol{F}^* = \boldsymbol{\xi}_1 \oplus \boldsymbol{\xi}_2 \oplus \cdots \oplus \boldsymbol{\xi}_C$. Then, construct a block diagonal design matrix $\mathbf{F}$, which is the Kronecker product of $\mathbb{I}_P$ and $\boldsymbol{F}^*$, $\mathbf{F} = \mathbb{I}_P \otimes \boldsymbol{F}^*$. Now estimate $\widetilde{\boldsymbol{\beta}} = [\mathbf{F}^T\mathbf{F}]^{-1}[\mathbf{F}^T\widetilde{\boldsymbol{\gamma}}]$.
Step 2. Using $\widetilde{\boldsymbol{\beta}}$ from Step 1, compute $\widetilde{\boldsymbol{R}} = \widetilde{\boldsymbol{\gamma}} - \widetilde{\boldsymbol{\beta}}$.
Step 3. Estimate $\widehat{\boldsymbol{\Sigma}}_\mathbf{b}$ by estimating the empirical variogram of $\widetilde{\boldsymbol{R}}$.
Step 4. Update $\widehat{\boldsymbol{\beta}} = [\mathbf{F}^T\widehat{\boldsymbol{\Sigma}}_\mathbf{b}^{-1}\mathbf{F}]^{-1}[\mathbf{F}^T\widehat{\boldsymbol{\Sigma}}_\mathbf{b}^{-1}\widetilde{\boldsymbol{\gamma}}]$.

Steps 2–4 are repeated until convergence, that is, the norm of the difference between current and updated values is less than 10^{-6}. The resulting naive estimator of $\mathbf{b}$ is $\widehat{\mathbf{b}} = \widetilde{\boldsymbol{\gamma}} - \widehat{\boldsymbol{\beta}}$.

3.2 Estimation of $\mathbb{C}\text{ov}(\mathbf{d}(\omega))$ and the Spectrum $f(\omega)$

As defined in Equation (6), $Z_{cv}(\omega) = Y_{cv}(\omega) - \boldsymbol{X}(\omega)[\boldsymbol{\beta}_c + \mathbf{b}_{cv}]$. Also, it can be seen that $Z_{cv}(\omega)$ can be expressed as $d_c(\omega) + \epsilon_{cv}(\omega)$. Using this relationship, it is possible to estimate the diagonal elements of the covariance matrix $\mathbb{C}\text{ov}(\mathbf{d}(\omega))$ as follows. Let $\widehat{\mathbb{C}\text{ov}}(A, B)$ denote the sample covariance between two random variables A and B, and $N(V_c)$ indicate the number of possible pairs of voxels in ROI c. For an ROI c, by the Weak Law of Large Number, the estimator

$$\widehat{\mathbb{V}\text{ar}}(d_c(\omega)) = [1/N(V_c)] \sum_{v \neq v'} \left\{ \widehat{\mathbb{C}\text{ov}}(Z_{cv}(\omega), Z_{cv'}(\omega)) \right\} \quad (9)$$

is unbiased for $\mathbb{V}\text{ar}(d_c(\omega)) = \sigma_{d_c}^2$ in Equation (6), that is, the average of the covariances of the Z_{cv}'s between any two voxels in ROI c is an unbiased estimator for $\sigma_{d_c}^2$.

The off-diagonal entries of $\mathbb{C}\text{ov}(\mathbf{d}(\omega))$ can be estimated by taking the average of the covariances of all possible pairs between two ROIs as discussed in Equation (5). This results in an unbiased estimator for the off-diagonal elements of the covariance matrix $\mathbb{C}\text{ov}(\mathbf{d}(\omega))$. For example, for ROIs c and c', when $c \neq c'$,

$$\begin{aligned}
\mathbb{C}\text{ov}(Y_{cv}(\omega), Y_{c'v'}(\omega)) &= \mathbb{C}\text{ov}(\boldsymbol{X}(\omega)\boldsymbol{\gamma}_{cv} + d_c(\omega) + \epsilon_{cv}(\omega), \\
&\quad \boldsymbol{X}(\omega)\boldsymbol{\gamma}_{c'v'} + d_{c'}(\omega) + \epsilon_{c'v'}(\omega)) \\
&= \mathbb{C}\text{ov}(d_c(\omega), d_{c'}(\omega)) \quad (10) \\
&\equiv \sigma_{d_{cc'}}^2,
\end{aligned}$$

where v and v' indicate any voxels in ROI c and c', respectively. Then the unbiased estimator for $\mathbb{C}\text{ov}(Y_{cv}(\omega), Y_{c'v'}(\omega))$ is

$$\widehat{\sigma}_{d_{cc'}}^2 = [1/(V_c \times V_{c'})] \sum_{i=1}^{V_c} \sum_{j=1}^{V_{c'}} \left\{ \widehat{\mathbb{C}\text{ov}}(Y_{ci}(\omega), Y_{c'j}(\omega)) \right\}. \quad (11)$$

It is natural to estimate the spectrum $f(\omega)$ by using the residuals after estimating $\mathbf{d}(\omega)$ in Equation (7). However, using the following relationship enables us to estimate the spectrum without estimating $\mathbf{d}(\omega)$: for any voxels v in ROI c,

$$\begin{aligned}
\mathbb{V}\text{ar}(Z_{cv}(\omega)) &= \mathbb{V}\text{ar}(Y_{cv}(\omega) - \boldsymbol{X}(\omega)\boldsymbol{\gamma}_{cv}) \\
&= \mathbb{V}\text{ar}(d_c(\omega) + \epsilon_{cv}(\omega)) \quad (12) \\
&= \sigma_{d_c}^2(\omega) + f(\omega).
\end{aligned}$$

Then, the spectrum at a frequency ω is $f(\omega) = \mathbb{V}\text{ar}(Z_{cv}(\omega)) - \sigma_{d_c}^2(\omega)$. Using Equation (9) and the sample variance of Z at a frequency ω, the spectrum for the real part is estimated

$$\widehat{f}^*(\omega) = [1/V_{\text{tot}}] \sum_{c=1}^{C} \sum_{v=1}^{V_c} \left\{ \widehat{\mathbb{V}\text{ar}}(Z_{cv}(\omega)) - \widehat{\sigma}_{d_c}^2 \right\}, \quad (13)$$

where $f^*(\omega) = (1/2)f(\omega)$, using only the real parts of $Z_{cv}(\omega)$ and $\widehat{\sigma}_{d_c}^2(\omega)$. However, using the imaginary parts also results in $\widehat{f}^*(\omega)$ because of the assumption $[\boldsymbol{\epsilon}^R(\omega), \boldsymbol{\epsilon}^I(\omega)]^T \sim N_{2V_{\text{tot}}}(\mathbf{0}, (1/2)f(\omega)\mathbb{I}_{2V_{\text{tot}}})$. Therefore, in the end, we can use the mean of the two $\widehat{f}^*(\omega)$'s (one calculated using the real parts and one calculated using the imaginary parts) as a more robust estimate for the spectrum $f(\omega)$. When considering a frequency band $\boldsymbol{\Omega}_\ell$ instead of a single frequency, we also need to average over all the frequencies that are elements of $\boldsymbol{\Omega}_\ell$.

3.3 Estimation of $\mathbb{C}\text{ov}(\widehat{\boldsymbol{\beta}})$

For performing any inference about a linear combination of $\boldsymbol{\beta}$, it is necessary to estimate the covariance of $\widehat{\boldsymbol{\beta}}$ in addition to the point estimates described above. The covariance of $\widehat{\boldsymbol{\beta}}$ can be estimated by using all the variance component estimates, $\boldsymbol{\Sigma}_\mathbf{b}$, $\boldsymbol{\Sigma}_\mathbf{d}(\omega)$, and $f(\omega)$. From Step 4 in Section 3.1,

$$\begin{aligned}
\mathbb{C}\text{ov}(\widehat{\boldsymbol{\beta}}) &= \mathbb{C}\text{ov}\left\{ [\mathbf{F}^T\widehat{\boldsymbol{\Sigma}}_\mathbf{b}^{-1}\mathbf{F}]^{-1}[\mathbf{F}^T\widehat{\boldsymbol{\Sigma}}_\mathbf{b}^{-1}\widetilde{\boldsymbol{\gamma}}] \right\} \\
&= [\mathbf{F}^T\widehat{\boldsymbol{\Sigma}}_\mathbf{b}^{-1}\mathbf{F}]^{-1}\mathbf{F}^T\widehat{\boldsymbol{\Sigma}}_\mathbf{b}^{-1}\mathbb{C}\text{ov}(\widetilde{\boldsymbol{\gamma}})\widehat{\boldsymbol{\Sigma}}_\mathbf{b}^{-1}\mathbf{F}[\mathbf{F}^T\widehat{\boldsymbol{\Sigma}}_\mathbf{b}^{-1}\mathbf{F}]^{-1},
\end{aligned}$$
$$(14)$$

where $\mathbb{C}\text{ov}(\widetilde{\boldsymbol{\gamma}})$ can be computed using Equation (8). It is obvious that

$$\begin{aligned}
\mathbb{C}\text{ov}(\widetilde{\boldsymbol{\gamma}}) &= \left[\sum_{i=1}^{M} \boldsymbol{X}^T(\boldsymbol{\Omega}_i)\boldsymbol{X}(\boldsymbol{\Omega}_i) \right]^{-1} \left[\sum_{i=1}^{M} \boldsymbol{X}^T(\boldsymbol{\Omega}_i)\boldsymbol{\Gamma}(\boldsymbol{\Omega}_i)\boldsymbol{X}(\boldsymbol{\Omega}_i) \right] \\
&\quad \times \left[\sum_{i=1}^{M} \boldsymbol{X}^T(\boldsymbol{\Omega}_i)\boldsymbol{X}(\boldsymbol{\Omega}_i) \right]^{-1} \\
&\equiv \boldsymbol{\Lambda},
\end{aligned}$$
$$(15)$$

where $\boldsymbol{\Gamma}(\boldsymbol{\Omega}_i) = \mathbb{V}\text{ar}(Y(\boldsymbol{\Omega}_i))$ as defined before. By combining Equation (14) with Equation (15), the covariance matrix of $\widehat{\boldsymbol{\beta}}$ is estimated as:

$$\widehat{\mathbb{C}\text{ov}}(\beta) = \left[\mathbf{F}^T\widehat{\boldsymbol{\Sigma}}_\mathbf{b}^{-1}\mathbf{F} \right]^{-1} \mathbf{F}^T\widehat{\boldsymbol{\Sigma}}_\mathbf{b}^{-1}\widehat{\boldsymbol{\Lambda}}\widehat{\boldsymbol{\Sigma}}_\mathbf{b}^{-1}\mathbf{F} \left[\mathbf{F}^T\widehat{\boldsymbol{\Sigma}}_\mathbf{b}^{-1}\mathbf{F} \right]^{-1}, \quad (16)$$

where $\mathbf{F}$ is defined in Step 1 in Section 3.1.

3.4 Inference

To answer the scientific question, "Which region(s) of interest in the brain is (are) activated when a certain type of stimulus is presented to a subject?," it is necessary to test hypotheses at each ROI while adjusting for multiple comparisons. For example, common hypotheses of interest that we are able to test are $H_0 : \beta_c^p - \beta_c^1 = 0$ at each ROI, where as before stimulus type "1" indicates the baseline condition. Our model and estimation described above yield the point estimates and covariance of $\widehat{\boldsymbol{\beta}}$ that enable us to compute t-statistics corresponding to the null hypothesis and perform inference about a linear combination of $\boldsymbol{\beta}$. It is important to emphasize that our modeling approach takes into account local spatial correlation as well as global correlation between any pairs of ROIs, yielding more accurate standard error estimates and reducing the chance of Type I errors. Of course, when there is more than one ROI of interest, it is still necessary to adjust for the multiple testing problem by employing one of many possible methods, for example, Bonferroni correction or False Discovery Rate (Benjamini and Hochberg 1995).

4. SIMULATIONS

We explored and validated our approach via simulation studies, where we generated spatially and temporally correlated time series with length 128 at each voxel. Then, we computed the error rate at an ROI for each method used to analyze the data. More details about data generation, methods, and comparisons are described below.

First, we assumed that there were five regions of interest that contain 100 voxels per ROI. At each voxel, we generated spatially and temporally correlated time series with length 128 using autoregressive model with order one (AR(1)) and exponential spatial covariance function. For the sake of simplicity, only two boxcar external stimuli were used for the mean signal. For the first set of simulation, the five ROIs were all assumed to be null ROIs, that is, $\beta_c^2 - \beta_c^1 = 0$, $c = 1, \ldots, 5$. However, for the second set of simulation, ROIs 4 and 5 were assumed to be nonnull ROIs, that is, $\beta_c^2 - \beta_c^1 \neq 0$.

To analyze the simulated data, we fitted a common general linear model employing AV-GLM. This approach only took into account the underlying temporal correlation using AR(1) model. In addition, three different models were employed to analyze the data: (1) our spatio-spectral model (SS), (2) the spatio-spectral model without taking into account the global correlation between ROIs (LSS), and (3) the spatio-spectral model without taking into account the local spatial correlation within a ROI (GSS). The hypothesis of interest was $H_0 : \beta_c^2 - \beta_c^1 = 0$ and $H_1 : \beta_c^2 - \beta_c^1 \neq 0$ at each ROI. We controlled the FDR at 0.05 to manage the multiple comparisons. For the first set of simulation, if any ROI was claimed to be significant, then it was counted as an error. For the second set of simulation, if any ROI among ROIs 1, 2, and 3 was claimed to be significant, or either ROI 4 or ROI 5 was not claimed to be significant, then it was counted as an error too. Tables 1 and 2 summarize the results for 500 repetitions for each set of simulation.

Each row corresponds to each method, that is, AV-GLM, SS, LSS, and GSS, and each column corresponds to each ROI in

Table 1. False positive error rates for the following approaches: standard approach (AV-GLM), spatio-spectral model (SS), spatio-spectral model without accounting for *global* correlation (LSS), and spatio-spectral model without accounting for *local* correlation (GSS) based on 500 simulations with $T = 128$ when all five ROIs were null

| Approach | False positive error rates | | | | | |
	ROI 1	ROI 2	ROI 3	ROI 4	ROI 5	Average
AV-GLM	0.88	0.89	0.88	0.89	0.88	0.88
SS	0.07	0.08	0.07	0.06	0.07	0.07
LSS	0.24	0.24	0.24	0.23	0.24	0.24
GSS	0.53	0.50	0.52	0.51	0.54	0.52

each table. The last column is for the average error rate for each method over ROIs. As shown in Table 1, when all the five ROIs are null, SS outperforms all the other approaches by showing the smallest error rate 0.07. This indicates that ignoring the underlying local and global correlations tends to inflate t-statistics and consequently makes more Type I errors. When there were two nonnull ROIs, AV-GLM works better than the others due to its strong tendency to reject the null hypothesis as shown in the columns for ROIs 4 and 5 in Table 2. However, AV-GLM shows higher error rates for the null ROIs, that is, higher false positives. The average error rate of SS is the smallest because its small loss in the error rates for ROIs 4 and 5 is well compensated by its ample savings in the error rates for ROIs 1 through 3. These two simulations empirically show that ignoring the underlying correlations in fMRI data results in much less reliable conclusions and our spatio-spectral model outperforms the other approaches that do not properly take into account the underlying correlations. We further fortify this claim by analyzing real fMRI data using both AV-GLM and SS models in Section 5.

5. ANALYSIS OF f MRI DATA

To identify brain activation patterns in a study designed to test cognitive control related activation in the prefrontal cortex (PFC) of the human brain, we used our proposed spatio-spectral mixed-effects model. Here, we describe the

Table 2. False positive (ROI 1 through ROI 3) and negative error rates (ROIs 4 and 5) for the following approaches: standard approach (AV-GLM), spatio-spectral model (SS), spatio-spectral model without accounting for *global* correlation (LSS), and spatio-spectral model without accounting for *local* correlation (GSS) based on 500 simulations with $T = 128$ when ROI 1 through ROI 3 were null but ROIs 4 and 5 were nonnull

| Approach | False positive rates | | | False negative rates | | |
	ROI 1	ROI 2	ROI 3	ROI 4	ROI 5	Average
AV-GLM	0.89	0.90	0.89	0.00	0.00	0.54
SS	0.14	0.14	0.14	0.06	0.05	0.10
LSS	0.30	0.29	0.30	0.01	0.02	0.18
GSS	0.47	0.46	0.45	0.13	0.12	0.33

background, motivation, and description of these data that are relevant to the current analysis of detecting patterns of activation and correlation in the functioning of the rostro-caudal axis of the frontal lobes.

Prior work (e.g., Long and Badre 2009; Badre and D'Esposito 2007) has demonstrated that the anterior premotor cortex (prePMd) is activated in an experimental situation where a subject selects one of two perceptual dimensions (i.e., shape or texture) of a stimulus that is relevant to then selecting a response. In the present experiment, participants were trained to associate four stimulus shapes with four keypress responses and four stimulus textures (e.g., webbed, streaked) with four keypress responses. Note that the response sets associated with shape and texture overlap and so making a correct response requires first selecting whether shape or texture is the relevant cue dimension. Thus, participants also learned to associate two colors with the shape dimension and two colors with the texture dimension. During the experiment, they would be presented a shape, shaded with a particular texture and surrounded by a colored box. Based on the color of the box, they would choose one of the four keypress responses based on either the associations they learned for shape or for texture.

Critically, for a given block of trials either one dimension would be cued throughout (D1) or two dimensions could be cued (D2). On D2 blocks, cognitive control is required to select the relevant dimension based on color. On D1 blocks, the same dimension is always relevant so minimal cognitive control is required. Based on prior work (Badre and D'Esposito 2007; Badre et al. 2009), the contrast of $D2 > D1$ should produce activation in prePMd. We term this region of interest ROI 1. Hierarchical theories of rostro-caudal frontal organization have suggested that regions rostral to prePMd (e.g., lateral frontal cortex, Brodmann area 9/46) are less likely to be activated by this specific control demand, but rather are involved in more abstract control (Koechlin, Ody, and Kouneiher 2003; Badre 2008). Thus, we also tested a region rostral to prePMd in lateral PFC close to that previously associated with higher order control (e.g., Badre and D'Esposito 2007); we term this ROI 2. Importantly, given the cortico-cortical connectivity of frontal cortex (Badre and D'Esposito 2009), though we do not predict a strong $D2 > D1$ effect in ROI 2, we do expect ROI 1 and ROI 2 to demonstrate functional connectivity, as they are both members of a common network. Finally, D2 versus D1 contrast is not predicted to reflect differences in low-level perceptual demands. Thus, we also defined an ROI in primary visual cortex (ROI 3) as an internal marker in which the $D2 > D1$ contrast is not expected to produce activation.

In the experiment, there were 288 trials, 144 of each dimension condition (D1, D2). Each trial lasted 2 sec, with a variable inter-trial interval of 0–8 sec. The trials were grouped into six scanning runs, with 48 trials per run. Each run is 4 min long and there are 4 blocks per run, 12 trials each, which follow an ABBA format for dimension type (e.g., D1, D2, D2, D1). The order of dimension condition is counterbalanced across subjects.

Whole-brain imaging was performed using the Siemens 3T TIM Trio MRI system at the Brown University MRI Research Facility. Functional images were acquired using a gradient-echo echo-planar sequence ($TR = 2$ sec; $TE = 30$ msec; flip angle $= 90$; 33 axial slices, $3 \times 3 \times 3.5$ mm). After the functional runs,

high-resolution T1-weighted (MP-RAGE) anatomical images were collected for visualization ($TR = 1900$ msec; $TE = 2.98$ sec; flip angle $= 9$; 160 sagittal slices, $1 \times 1 \times 1$ mm). Head motion was restricted using firm padding that surrounded the head. Visual stimuli were projected onto a screen and viewed through a mirror attached to a matrix eight-channel head coil.

Preprocessing and data analysis were performed using SPM2 (*http://www.fil.ion.ucl.ac.uk/spm/*) and MATLAB (MathWorks, Natick, MA). Following quality assurance procedures to assess outliers or artifacts in volume and slice-to-slice variance in the global signal, functional images were corrected for differences in slice acquisition timing by resampling all slices in time to match the first slice. Images were then motion corrected across all runs. Functional data were then normalized based on Montreal Neurological Institute stereotaxic space but were not spatially smoothed.

We used Model (3) to the data collected from a single subject to see if we could find any activated ROI(s) among three given ROIs in which there are 20 voxels per ROI. The model contains only three covariates, which are for D1, D2, and the instruction period (IP). The three stimuli are convolved with the canonical HRF used in SPM2 and are denoted by X_{D1}, X_{D2}, and X_{IP}, respectively. The corresponding regression coefficients are β_c^{D1}, β_c^{D2}, and β_c^{IP} in ROI c, where $\beta_c^{D2} - \beta_c^{D1}$ is of main interest to test the hypothesis, $H_0 : \beta_c^{D2} \geqq \beta_c^{D1}$, $c \in \{1, 2, 3\}$. In this analysis, two frequency bands are used: lower frequency, 0.07–0.12 Hz; and higher frequency, 0.15–0.20 Hz. The approximate band segmentation was justified by the work of Curtis et al. (2005), although the band segmentation still depends on subjective decision. The *local* spatial covariance matrices within each ROI and *global* covariance matrix among ROIs were estimated following the procedures in Sections 3.1 and 3.2. Given the point estimates and covariance of $\beta^{D2} - \beta^{D1}$ at each ROI, *p*-values were computed based on *t*-statistics and ROIs were evaluated for their statistical significance while controlling the FDR at the level of 0.1.

The point estimates with their standard errors and corresponding *p*-values based on one-sided test at ROIs are illustrated in Table 3. The difference in blood-oxygen-level dependence (BOLD) signals due to the two external stimuli is the most significant in the rostral sector of the dorsal premotor cortex (prePMd) area (ROI 1), while it is also significant in lateral PFC (ROI 2), after controlling FDR at 0.1. To investigate the difference between our model and a standard approach, we also analyzed the data using AV-GLM. The *p*-values corresponding to ROIs 1, 2, and 3 are < 0.01, < 0.01, and 0.10, which are all claimed as active at FDR $= 0.1$. Because D2 versus D1 contrast is not expected to reflect differences in ROI 3 as described before, it can be concluded that ignoring the local spatial

Table 3. Point estimates of $\beta_c^{D2} - \beta_c^{D1}$, estimated standard errors (SE) of point estimates, and *p*-values associated with one-sided test at ROIs

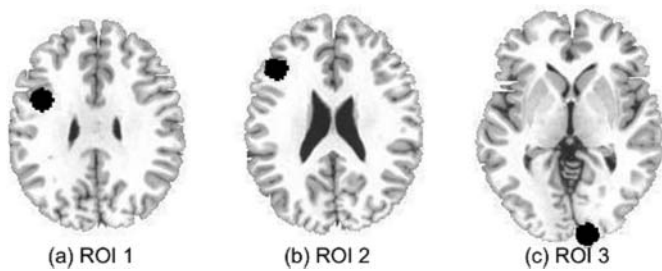|	Point estimate	SE	*p*-value
ROI 1	0.98	0.61	0.05
ROI 2	0.63	0.40	0.06
ROI 3	−0.35	0.26	0.91

Figure 2. Black dots on the axial slices of the brain illustrate the three ROIs; their coordinates are also included : (a) ROI 1 $(-40, 4, 30)$, (b) ROI 2 $(-42, 28, 24)$, and (c) ROI 3 $(14, -100, 0)$.

correlation and global correlation in fMRI data results in misleading scientific findings. This result is consistent with our claim supported via simulation studies in Section 4, that is, t-statistics are inflated with ignored underlying positive correlation.

The three ROIs are illustrated in Figure 2, where ROI 1, ROI 2, and ROI 3 are denoted by black dots in each axial slice of the brain image. Their x-, y-, and z-coordinates in the brain are also included, where the origin is at the center of the brain. In Figure 3, the *global* correlation among the three ROIs is summarized using heat maps, in which a lighter color indicates higher correlation and darker colors indicate lower correlation. Even though we do not formally test for statistical significance of the correlation between any two ROIs, within both the real and imaginary parts, it appears that the correlation between ROIs 1 and 2 is higher than any of the other pairwise correlations over all frequency bands. The suggested functional coupling between prePMd (ROI 1) and lateral PFC (ROI 2) is consistent with the known neuroanatomy. More importantly, the results provide further empirical evidence supporting the novel hypothesis that these structures along the rostro-caudal axis are part of a functional network (Badre and D'Esposito 2009). Understanding

the functional organization is fundamental to comprehending frontal lobe function, which can shed light on the association between focal brain damage in this region and impaired ability of making some action decision. Some of the behavior disorders include attention disorder, poor memory, diminution of spontaneous activity, and sensory inattention. Also, it is known that schizophrenia and dementia can result from frontal lobe abnormalities. Therefore, it is critical to understand frontal lobe function, frontal lobe abnormalities, and characteristics of the behavior disorders for diagnosis and prognosis of the mental disorders.

6. CONCLUSION

To overcome the main barrier of fitting spatio-temporal model in fMRI data analysis, we propose a spatio-spectral model that reveals the essential features of fMRI data. Our model consists of the fixed and random terms that capture ROI-specific fixed effects due to external stimuli, temporal correlations, and multiscale spatial correlations. The covariance structure in the frequency domain is much simpler than that in time domain, which significantly reduces the computational burden of simultaneously estimating the temporal and spatial correlation typically present in fMRI data. In practice, when the scientists have predetermined regions of interest, computational cost in fitting spatio-spectral models is further minimized. Our model can be used to determine active ROI(s) not by looking at each voxel separately, but by pooling information from all the voxels in each ROI as well as taking into account *global* correlation between ROIs. In our model, although we assume that each voxel within an ROI shares the same mean response, that is, functional homogeneity, it would be unrealistic to assume the homogeneity of the variance of the mean response estimator due to the spatio-temporal random effects. Therefore, declaring an ROI to be active does not necessarily imply that all voxels within the ROI are active. Conversely, it is possible that an ROI having a relatively small proportion of active voxels would not be declared active. Although this might be argued to be a limitation of our model, it is not obvious whether or not an ROI having only one or very few active voxels should be claimed active, and to our knowledge there are no practical guidelines on this issue.

Our model requires estimating spatial correlation, which is quite different from employing spatial smoothing. While the objective of both approaches is to take into account intrinsic spatial correlation among voxels, our model tries to estimate the correlation as opposed to using spatial smoothing, which introduces another type of spatial correlation on top of underlying spatial correlation. Spatial smoothing may be more computationally efficient, but in terms of flexibility and inference, our approach is believed to outperform spatial smoothing methods. Specifically, when there is a negative-valued correlation between two ROIs, our model can capture it via an ROI-specific random term, while this would not be possible in other common approaches based on spatial smoothing. Consequently, we can argue that inference about regression coefficients based on our model tends to be less biased compared to spatial-smoothing approaches. Nonparametric estimation of the local spatial covariance matrix enables us to properly and naturally handle nonstationarity of spatial correlation. Moreover, allowing ROI-specific random
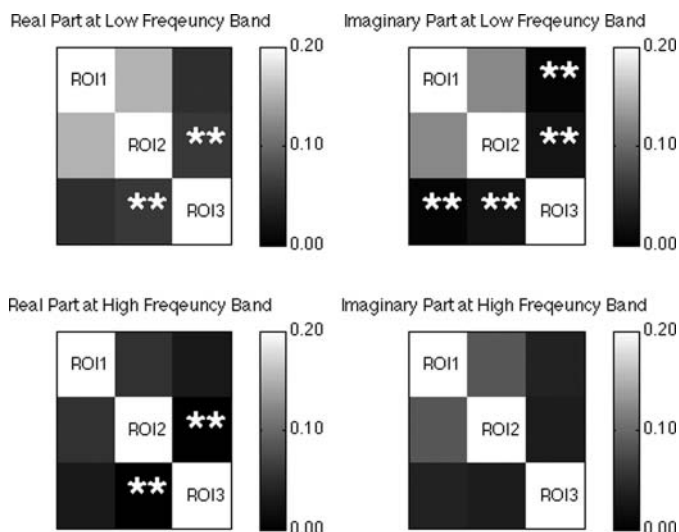

Figure 3. Heat map for the absolute values of correlations among the three ROIs. The two maps on the first column are for real part at low and high frequency bands, while those on the second column are for imaginary part at low and high frequency bands. Negative correlation is denoted by **.

effects at different frequency bands disentangles the interaction between spatial and temporal correlations, which would not be easily dealt with in other approaches.

The model described in Bowman (2007) and our spatio-spectral model shares similarities and dissimilarities. The two models try to avoid spatial smoothing not to capture spatial dependency in neuroimaging data, but rather to *model* the spatial dependency. The most distinct difference between the models is that our model operates in the frequency domain while the Bowman's model operates in the time domain. Moreover, the lack of appreciating the between-ROI *global* correlation in the Bowman's model makes it very different from our model. The LSS approach discussed in Section 4 would be similar to the Bowman's model in terms of not considering *global* correlation. However, it is not feasible to conclude that our model outperforms the Bowman's model only based on the simulation studies.

One limitation of our model is the isotropic assumption described in Section 2.2. If the size of an ROI is large, then it might be unrealistic that the underlying spatial process in the ROI is isotropic. However, we assessed the validity of the assumption by visual inspection of four different directional empirical variograms. Based on the similarity of the four variograms, we think that the isotropic assumption in our data analysis is reasonable. Another potential limitation is the stationarity assumption of the noise, $\epsilon_{cv}(t)$. One potential extension of our model to properly handle nonstationary time series is to employ the wavelet transformation as described in Nason, von Sachs, and Kroisandt (2000); Bullmore et al. (2001), where the stationarity assumption is no longer required. Although we used nonparametric empirical variograms to capture the within-ROI spatial correlation, it may be advantageous to assume a parametric spatial correlation instead of using empirical variogram in terms of computational burden as the number of voxels in an ROI increases. For the between-ROI correlation, it would be advantageous to impose a parametric covariance function to estimate the *global* correlation if there is relatively large number of ROIs. However, it will require more complex model to capture a negative-valued correlation, for example, a linear combination of two valid covariance functions (Gregori et al. 2008).

[Received August 2010. Revised December 2011.]

REFERENCES

Badre, D. (2008), "Cognitive Control, Hierarchy, and the Rostro-Caudal Axis of the Prefrontal Cortex," *Trends in Cognitive Science*, 12, 193–200. [574]

Badre, D., and D'Esposito, M. (2007), "FMRI Evidence for a Hierarchical Organization of the Prefrontal Cortex," *Journal of Cognitive Neuroscience*, 19, 2082–2099. [574]

——— (2009), "Is the Rostro-Caudal Axis of the Frontal Lobe Hierarchical?," *Nature Reviews Neuroscience*, 10, 659–669. [574,575]

Badre, D., Hoffman, J., Cooney, J. W., and D'Esposito, M. (2009), "Hierarchical Cognitive Control Deficits Following Damage to the Human Frontal Lobe," *Nature Neuroscience*, 12, 515–522. [574]

Benjamini, Y., and Hochberg, Y. (1995), "Controlling the False Discovery Rate: A Practical and Powerful Approach to Multiple Testing," *Journal of Royal Statistical Society*, Series B, 57, 289–300. [572]

Bowman, F. D. (2005), "Spatio-Temporal Modeling of Localized Brain Activity," *Biostatistics*, 6, 558–575. [568]

——— (2007), "Spatiotemporal Models for Region of Interest Analyses of Functional Neuroimaging Data," *Journal of the American Statistical Association*, 102, 442–453. [568,576]

Bowman, F. D., Caffo, B., Bassett, S. S., and Kilts, C. (2008), "A Bayesian Hierarchical Framework for Spatial Modeling of fMRI Data," *NeuroImage*, 39, 146–156. [569]

Brockwell, P. J., and Davis, R. A. (1991), *Time Series: Theory and Methods* (2nd ed.), New York: Springer, chap. 10. [570]

Bullmore, E., Brammer, M., Williams, S. C. R., Rabe-Hesketh, S., Janot, N., Daivd, A., Mellers, J., Howard, R., and Sham, P. (1996), "Statistical Methods of Estimation and Inference for Functional MR Image Analysis," *Magnetic Resonance in Medicine*, 35, 261–277. [568]

Bullmore, E., Long, C., Suckling, J., Fadili, J., Calvert, G., Zelaya, F., Carpenter, T. A., and Brammer, M. (2001), "Colored Noise and Computational Inference in Neurophysiological (fMRI) Time Series Analysis: Resampling Methods in Time and Wavelet Domains," *Human Brain Mapping*, 12, 61–78. [568,576]

Carlin, B. P., and Banerjee, S. (2003), "Hierarchical Multivariate CAR Models for Spatio-Temporally Correlated Survival Data," in *Bayesian Statistic 7*, eds. J. M. Bernado, M. J. Bayarri, J. O. Berger, A. P. Dawid, D. Heckerman, A. F. M. Smith, and M. West, Oxford: Oxford University Press, pp. 45–63. [569]

Chilès, J. P., and Delfiner, P. (1999), *Geostatistics: Modeling Spatial Uncertainty*, New York: Wiley. [569,571]

Cressie, N. (1993), *Statistics for Spatial Data*, New York: Wiley. [571]

Curtis, C. E., Sun, F. T., Miller, L. M., and D'Esposito, M. (2005), "Coherence between fMRI Time-Series Distinguishes Two Spatial Working Memory Networks," *NeuroImage*, 26, 177–183. [574]

Dubin, R. A. (1988), "Estimation of Regression Coefficients in the Presence of Spatially Autocorrelated Error Terms," *Review of Economics and Statistics*, 70, 466–474. [568]

Genovese, C. R. (2000), "A Bayesian Time-Course Model for Functional Magnetic Resonance Imaging Data," *Journal of the American Statistical Association*, 95, 691–703. [569]

Gregori, P., Porcu, E., Mateu, J., and Sasvári, Z. (2008), "On Potentially Negative Space Time Covariances Obtained as Sum of Products of Marginal Ones," *Annals of the Institute of Statistical Mathematics*, 60, 865–882. [576]

Huettel, S. A., Song, A. W., and McCarthy, G. (2004), *Functional Magnetic Resonance Imaging*, SunderlandMA: Sinauer Associates, chap. 10. [568]

Katanoda, K., Matsuda, Y., and Sugishita, M. (2002), "A Spatio-Temporal Regression Model for the Analysis of Functional MRI Data," *NeuroImage*, 17, 1415–1428. [568,570]

Koechlin, E., Ody, C., and Kouneiher, F. (2003), "The Architecture of Cognitive Control in the Human Prefrontal Cortex," *Science*, 302, 1181–1185. [574]

Lange, N., and Zeger, S. L. (1997), "Non-Linear Time Series Analysis for Human Brain Mapping by Functional Magnetic Resonance Imaging," *Applied Statistics*, 46, 1–29. [568,570,571]

Lazar, N. A. (2008), *The Statistical Analysis of Functional MRI Data*, New York: Springer, chap. 6. [570]

Locascio, J. J., Jennings, P. J., Moore, C. I., and Corkin, S. (1997), "Time Series Analysis in the Time Domain and Resampling Methods for Studies of Functional Magnetic Resonance Brain Imaging," *Human Brain Mapping*, 5, 168–193. [568]

Long, N. M., and Badre, D. (2009), "Testing Hierarchical Interactions in Frontal Cortex During Cognitive Control," Poster presented at the 16th Cognitive Neuroscience Society meeting. [574]

Muller, K., Lohmann, G., Bosch, V., and Von Cramon, D. (2001), "On Multivariate Spectral Analysis of fMRI Time Series," *NeuroImage*, 14, 347–356. [569]

Nason, G. P., von Sachs, R., and Kroisandt, G. (2000), "Wavelet Processes and Adaptive Estimation of the Evolutionary Wavelet Spectrum," *Journal of the Royal Statistical Society*, Series B, 62, 271–292. [576]

Ombao, H., Shao, X., Rykhlevskaia, E., Fabiani, M., and Gratton, G. (2008), "Spatio-Spectral Analysis of Brain Signals," *Statistica Sinica*, 18, 1465–1482. [568]

Rowe, D. (2005), "Modeling both the Magnitude and Phase of Complex-Valued fMRI Data," *NeuroImage*, 25, 1310–1324. [568]

Shumway, R. H., and Stoffer, D. S. (2006), *Time Series Analysis and Its Application with R Examples* (2nd ed.), New York: Springer, pp. 543–544. [570,571]

Sun, F. T., Miller, L. M., and D'Esposito, M. (2004), "Measuring Interregional Functional Connectivity Using Coherence and Partial Coherence Analysis of fMRI Data," *NeuroImage*, 21, 647–658. [569]

Worsley, K., and Friston, K. (1995), "Analysis of fMRI Time Series Revisited – Again," *NeuroImage*, 2, 173–181. [568]

Worsley, K. J., Evans, A. C., Marrett, S., and Neelin, P. (1992), "A Three-Dimensional Statistical Analysis for rCBF Activation Studies in the Human Brain," *Journal of Cerebral Blood Flow and Metabolism*, 12, 900–918. [568]

Worsley, K. J., Liao, C. H., Aston, J., Petre, V., Duncan, G. H., Morales, F., and Evans, A. C. (2002), "A General Statistical Analysis for fMRI Data," *NeuroImage*, 15, 1–15. [568]

Worsley, K. J., Marrett, S., Neelin, P., Vandal, A. C., Friston, K. J., and Evans, A. C. (1996), "A Unified Statistical Approach for Detecting Significant Signals in Images of Cerebral Activation," *Human Brain Mapping*, 4, 58–73. [568]

Yue, Y., Loh, J. M., and Lindquist, M. A. (2010), "Adaptive Spatial Smoothing of fMRI Images," *Statistics and Its Interface*, 3, 3–13. [569]

Zhu, H., Li, Y., Ibrahim, J. G., Shi, X., An, H., Chen, Y., Gao, W., Lin, W., Rowe, D. B., and Peterson, B. S. (2009), "Regression Models for Identifying Noise Sources in Magnetic Resonance Images," *Journal of the American Statistical Association*, 104, 623–637. [568]